Peer Reviewed
2017 Solar Research Conference

In-situ, well-resolved planar temperature measurement of radiatively-heated particles

Kimberley C.Y. Kueh[1], Timothy C.W. Lau[1], Graham J. Nathan[1] and Zeyad T. Alwahabi[2]

[1] *School of Mechanical Engineering, The University of Adelaide, North Terrace, Adelaide 5005, Australia.*
[2] *School of Chemical Engineering, The University of Adelaide, North Terrace, Adelaide 5005, Australia.*
E-mail: kimberley.kueh@adelaide.edu.au

Abstract

A direct, single-shot, non-intrusive planar temperature measurement of micron-sized particles in an unsteady flow has been demonstrated. Particles of diameters between 10µm and 50µm were fluidised using an optically-accessible fluidised bed system. The particle temperature was measured with a single ICCD camera fitted with an image splitter and filters to simultaneously record two images over a 7.5mm × 10.8mm area. This resulted in particle temperature maps of 51 pixels/mm, with an average of 15 particles in the measurement region at any given time. The particles were heated to temperatures up to 350°C with solid-state solar thermal simulator to generate a highly uniform heating region at fluxes of up to 21.1 MW/m^2. These fluxes exceed the range typically found in the particle receivers in Concentrated Solar Thermal (CST) systems, demonstrating that the method is more suitable for investigating heat transfer in them.

1. Introduction

Concentrated solar thermal (CST) technology is receiving ongoing investment due to the abundance of the solar resource and its potential for large-scale power generation, low cost energy storage, and hybridisation (Denholm et al., 2013; Gil et al., 2010; Kuravi et al., 2013). Solar particle receivers/reactors are among CST technologies under develpment because of their potential to achieve higher temperature than is possible with current CST technologies that utilises molten salt, air, or mineral oils (Grena, 2009) and thereby lower overall costs. Of the various types of receiver, those that employ direct irradiation from the concentrated solar irrdiation achieve highly effecient heat transfer to small particles. However, there is a need to ramp up the development of these technologies both because of the ongoing ned to lower costs (Kreith and Goswami, 2007) and because of the need for schedulable renewable generators in the emerging networks(IEA, 2014). The work that is currently being undertaken to increase the thermal efficiencies of solar particle receivers (Chen et al., 2006; Grena, 2009; Wang et al., 2016) is limited by the lack of a comprehensive understanding of fundamental heat transfer processes involved in such systems. This is because the process of heat transfer within these receivers is highly complex, with combined effects of particle-fluid coupling, inter-particle interactions, particle clustering and more (Lau and Nathan, 2016; Lau and Nathan, 2017; Monchaux et al., 2012). However, the pursuit of underderstanding these processes is, in turn, limited by the lack of suitable methods with which to perform well-resolved, in-situ measurement of the relevant parameters n the challenging environmen of particle-laden flows. One such measurement for which new methods are needed is that of the temperature of particles

suspended in a turbulent flow and subjected to radiative heating. The present paper is directed to meet this need.

With the advancement of laser diagnostics, a technique that allows for the direct planar measurement of particle temperatures has been developed. A special type of particles, known as thermophosphors (TP), are suitable for laser-induced phosphorescent (LIP) measurement due to their combined properties of being to survive high temperature environments, being chemically inert and emitting a temperature-dependent phosphorescent signal. A key advantage of the LIP technique is that it is applicable to a wide range of temperature ranges due to a wide range of TPs available, each with its own operating temperature range and decaying lifetime. A comprehensive review of this has been compiled by Aldén et al. (2011). For the present investigation, the particle temepratures are not expected to reach 600°C. As such, ZnO:Zn is used, as it has the highest sensitivity at the operating temeprature range (Särner et al., 2008). However, previous applications of LIP has been for the measurement of gas-phase temperatures. To achieve this, micron-sized TPs are seeded as tracers into the flow and assumed to be at thermal equilibrium with it (Abram et al., 2015; Fond et al., 2012; Hasegawa et al., 2007; Jovicic et al., 2015). However, the assumption is not valid in conditions of high radiation fluxes such as occurs in solar receivers, which we estimate can generate heating rates on the order of 10,000°C/s. To investigate heat transferin these conditions, it is necessary to emply a heat souce with sufficiently high irradiative heat flux that is also very well-characterised and, preferably, uniform.

The present investigation employs a well-characterised solid-state radiation source that has recently been developed to deliver well-characterised radiative heat fluxes of up to 36.6 MW/m^2 (Alwahabi et al., 2016). This has been employed in an optically-accessible fluidised bed to achieve heating rates of up to 23,000°C/s (Kueh et al., 2017). Additionally, it operates at a peak wavelength of 910nm that is absorbed only by the particle phase and not by air. As distinct from previously used radiative heat sources such as deuterium and tungsten lamps, this Solid-State Solar Thermal Simulator (SSSTS) does not generate hot-spots in which certain heating region is higher than others and has a near top-hat beam profile. Hence, the aim of the present investigation is demonstrate a direct, in-situ planar temperature measurement of unsteady particles heated by a well-characterised radiative heat source.

2. Experimental

2.1. Optical Arrangement

The optical arrangement is presented in Fig. 1. Here, ZnO:Zn thermophosphors (TPs, Phosphor Technology) are suspended in air within an optically-accessible fluised bed, FB, and excited by a third harmonic of an Nd:YAG (Quantel Q-smart 850) laser operated at 5.27 ± 0.47mJ and 355nm (shown in purple in Fig. 1). The TP particles have a a size distribution of 1µm-50µm. However, to avoid agglomeration, these were mixed with non-phosphorescent $CaSO_4 \cdot 2H_2O$ particles of 100µm-200µm at a ratio of 20:80. This approach follows the earlier work of Abram et al. (2013). Three cylindrical lenses (L_1, L_2, L_3) were used in series to manipulate the 355nm laser beam and generate a 10.5mm wide by 300µm thick laser sheet at the measurement test secton to excite the TPs. The subsequent phosphorescent emissions (shown as dotted lines in Fig. 1) were then recorded with an ICCD camera (PI-Max/PI-Max2 - Princeton Instruments) through a 40mm spacer (sp) and an f/2.8 Tamron imaging lens (ImL). Images collected with the ICCD camera fitted with an image splitter (Opto-Split II - Cairns Research, IS) resulted in a single image divided in half, where one half was taken with a high transmission filter (FF01-

440/40-25, Semrock) at bandwidth LP420 ± 20nm and the other (FF01-440/40-25, Semrock) at 392 ± 9nm. Each of the sub-images views the same 15mm × 10.5mm area simultaneously, thus minimizing time-delay and angular distortion errors typical of using traditional two-camera systems. The camera gain, gate width and gate delay were set to 5, 26ns and 51ns respectively, to maximize the phosphorescence signal collection. To heat the particles, the Solid-state Solar Thermal Simulator (SSSTS, shown in red in Fig. 1) beam path is aligned 7° from the 355nm laser path such that they intercept in the centre of the FB chamber. A beam splitter (BS) is used to split the SSSTS beam into a ratio of 92:8. Two water-cooled power meters (PM_1, PM_2) were used to measure the power of the SSSTS and act as beam dumps to the heating beams. To relate phosphorescent emssions to temperature, a calibration experiment was performed with the same experimental setup described, with the exception that a TP-coated plated in a temperature-controlled oven is located in place of the FB.

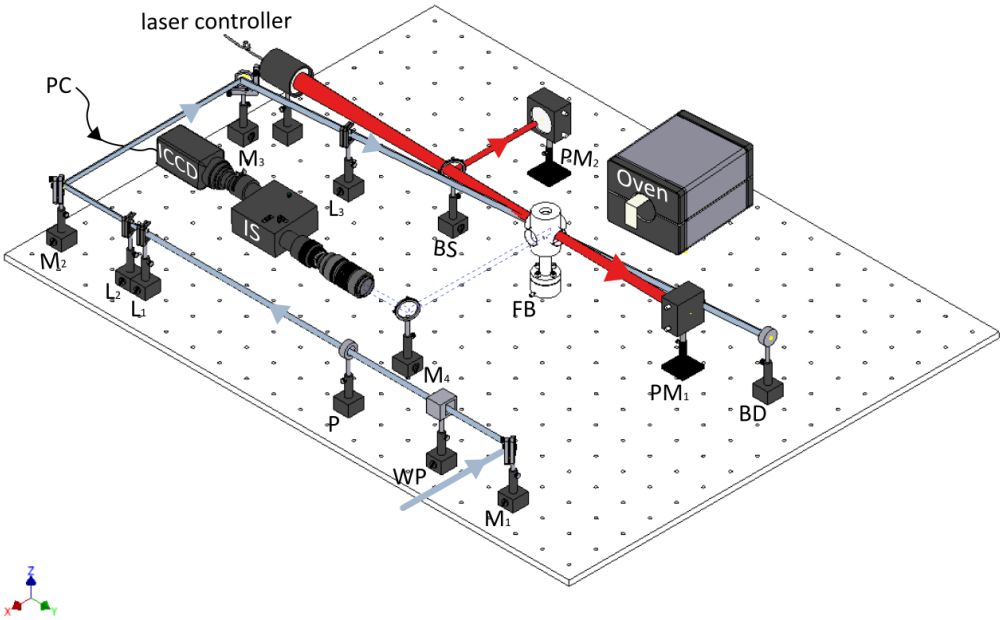

Fig. 1. Optical arrangement. Note that the temperature-controllable oven replaces the fluidized bed during calibration. Purple line: 355nm Nd:YAG laser beam path; Red line: 910nm Solid-State Solar Thermal Simulator (SSSTS) beam path; Blue dashed line: optical collection path of phosphorescence emission. BD: Beam Dump; BS: Beam Splitter; FOC: Fibre-optic Cable; ImL: Imaging Lens; L: Lens; M: Mirror; P: Polariser; PM: Power Meter; sp: spacer; WP: Waveplate.

2.2. Methodology

2.2.1. Temperature Calibration

Calibration of the ZnO:Zn phosphorescent emissions was performed by systematically increasing the temperature of the TP-coated plate in the oven between 22°C and 425°C. For each temperature, the plate was allowed to reach thermal equilibrium before measurements were taken. At each temperature, 100 images were recorded for each measurement set and the intensity ratio calculated. The intensity ratios, along with the error range, were then plotted against temperature to be used as a calibration curve.

2.2.2. Temperature measurement of fluidised particles

Fluidised particles were subjected to systematic radiative heating by the SSSTS and excitation of the 355nm Nd:YAG laser. 14 sets of measurements were performed with heat fluxes, Φ, between 2.4 MW/m^2 and 21.1 MW/m^2. In each set of measurement, 800 single-shots images

were taken, the first and last 50 shots taken with no irradition, and 650 shots with the SSSTS switched on. Recorded images were then processed via in-house codes on Matlab. Given that an image splitter was used in conjuction with the ICCD camera, a single image divided in half, where one half of it is taken with the LP420 ± 20nm filter and the other with the 392 ± 9nm filter, is obtained for every measurement. These sub-images were then superpositioned and divided against pixel-by-pixel to obtain a arrays of intensity ratios. A correspponding temperature image can then be inferred from the calibration curve. Given that laser fluence has a tendency to influence phosphorescent emission (Abram et al., 2015), the intensity ratio is divided against that of a reference case at room temperature.

At the same time, power measurements from both the power meters (PM_1, PM_2 in Fig. 1) were recorded to estimate radiation attenuation by the particles, $\dot{Q}_{att}$. This value was calculated by taking the difference between the two power meter readings after correcting for differences in beam power due to the beam splitter, i.e. $\dot{Q}_{att} = \dot{Q}_{in} - \dot{Q}_{out}$, where $\dot{Q}_{in}$ is the power recorded by PM_1 multiplied by 100/92, and $\dot{Q}_{out}$ is the power recorded by PM_2, multiplied by 100/8.

3. Results and Discussion

Fig. 2 presents the calibration of phosphorescence emission with respect to temperature. The intensity ratio was calculated through image processing where image pairs taken with filters at bandwidth 440 ± 20nm and 392 ± 9nm were superpositioned and divided against each other. The calibration was performed multiple times and was found to be highly repeatable, with an accuracy within ±4%.

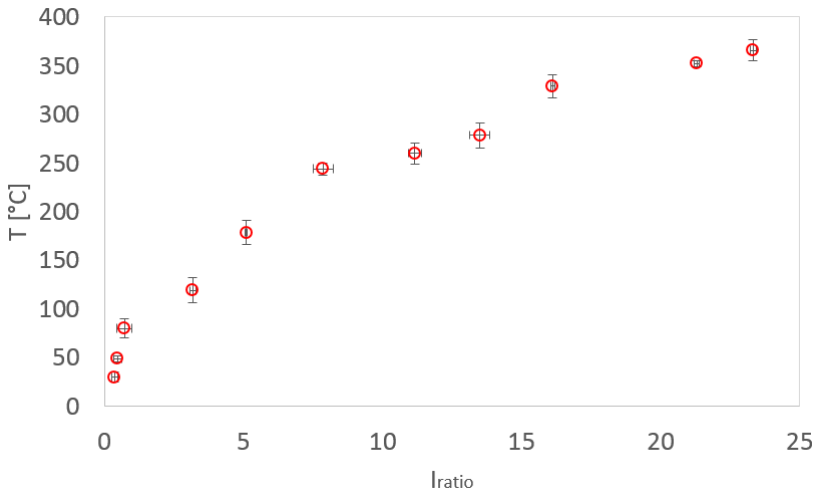

Fig. 2: Calibration curve relating phophorescent emission of ZnO:Zn to temperature, where intensity ratio was calculated by superpositioning and dividing images taken with filters at 440 ± 20nm and 392 ± 9nm.

Fig. 3 presents examples of particle images heated at five alternative values of flux: (1) 0 MW/m^2 and (2) 12.4 MW/m^2. Columns A and B corresponds to the individual raw images of a particle agglomerate collected at the two wavelengths of 420nm ± 20 (FF01-440/40-25) and 392 ± 9nm (FF01-392/18-25) respectively, while column C shows the image of the resultant inferred particle temperature, T_p, derived from the calibration curve. As it can be seen, the image intensities of the particle agglomerate taken with the 420nm ± 20 filter can be seen to increase with heat flux, while the opposite is true for those taken with the 392 ± 9nm filter. This is consistent with the spectra shift presented by Särner et al. (2008). It should also be noted that the scatter in the range of measurements for particles are ranfom, consistent with the CCD noise from particles in thermal equilibrium, as expected from Biot number calculations of

particles in thesre size range (Kueh *et.al.* 2017). Hence, the mean particle temperature can be derived with low noise by averaging all of the pixels for a given particle.

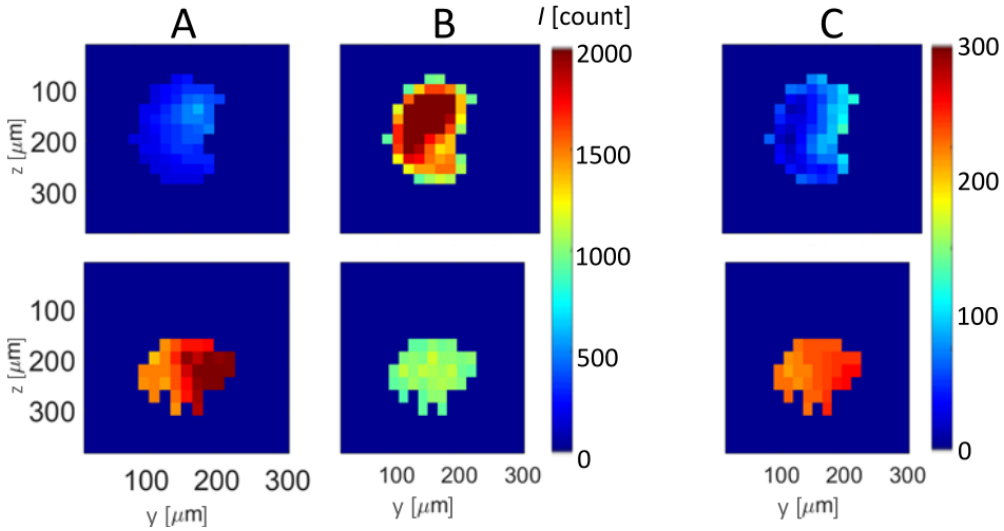

Fig. 3: Typical examples of image trios of particle agglomerates, comprising raw image pairs 420 ± 20nm (column A) and at 392 ± 9nm (column B), together with the resulting temperature, T_p (column C), recorded for five values of radiative heat flux, Φ: (1) 0 MW/m^{2}and (2) 12.4 MW/m^2.

Fig. 4 presents the probability distribution of T_p calculated from all particles, $T_{p,all}$, over 650 captured images when the heat flux was set to 12MW/m^2, as well as temperature of 3 single particles (T_{p1}, T_{p2}, T_{p3}). It can be seen that particle temperature change in the range of ±5% to ±10% was detected for individual particle aggolmerates, as well as the overall particle agglomerate distribution. This is in line with the findings presented in Fig. 2, and distribution can be attributed to noise from the two ICCD images, rather than to any actual temperature variations within the particles due to the low Biot number.

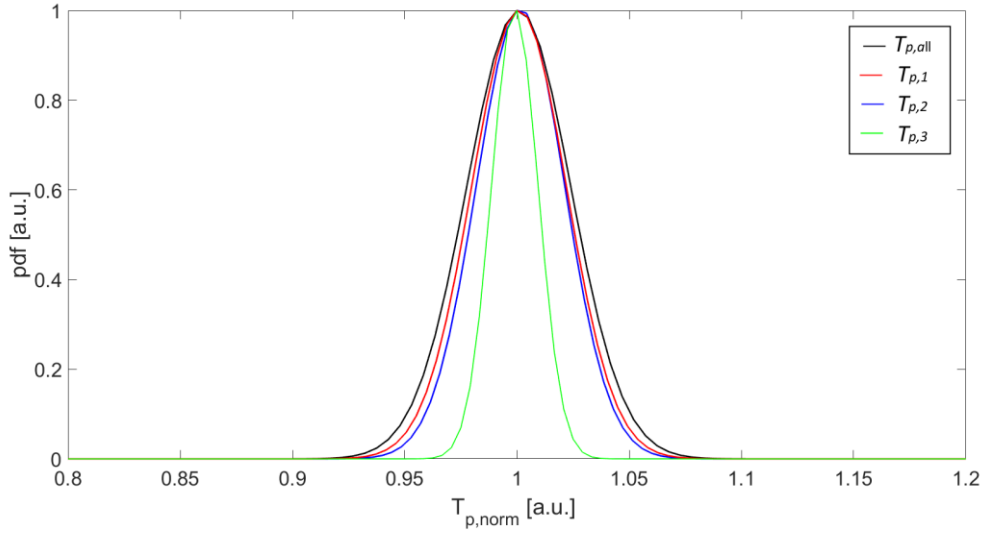

Fig. 4: Probability distribution comparison of particle temperatures, T_p, where $T_{p,all}$ was calculated based on all T_p over 650 captured images, while T_{p1}, T_{p2}, T_{p3} are the temperatures of single particles.

Fig. 5 presents selected individual particle temperatures as a function of their location with respect to the heating and excitation lasers at Φ = 0 MW/m^2, 3.34 MW/m^2, 12.4 MW/m^2, and 21.1 MW/m^2. The mean temperature of all particles within the 650 captured images were first tabulated with respect to their core location before the mean particle temperatures at selected

locations were plotted in the present figure. Here, the errorbars denotes the standard deviation of the particle temperatures at the particular location. The heating and excitation source direction is plotted in the *y*-direction (as presented in the coordinate in Fig. 1). A comparison of TPs heated at fluxes 0MW/m^2 to 21.1.MW/m^2 shows significant increase in T_p despite the short residence time in the heating sheet (determined by setting exposure time of ICCD camera to 3ms and calculating particle travel path length).

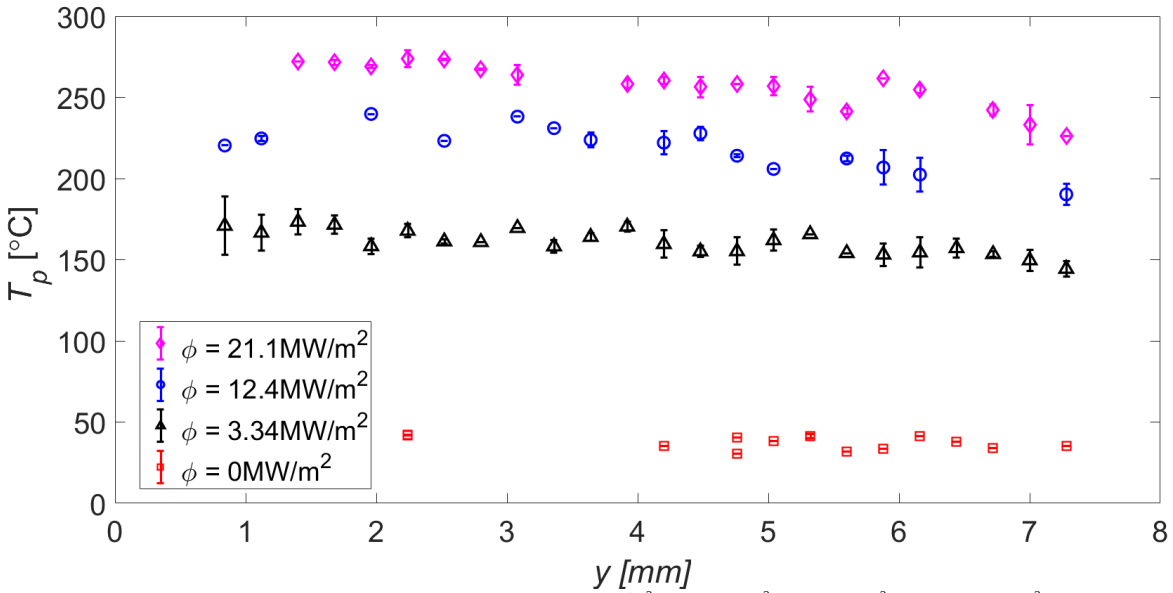

Fig. 5: Selected particle temperature heated at Φ = 0 MW/m^2, 3.34 MW/m^2, 12.4 MW/m^2, and 21.1 MW/m^2.

Fig. 6 presents the mean temperatures of all particles within an image and the corresponding number of particles per image for Φ = 2.4 MW/m^2, 107 MW/m^2, 12.4 MW/m^2 and 21.1. MW/m^2. As can be seen, there is a strong correlation between particle mass loading and the local (instantaneous) mean particle temperature within the volume. Since the Φ is constant for a given experimental run, this strong correlation implies that inter-particle heat transfer is significant in this system.

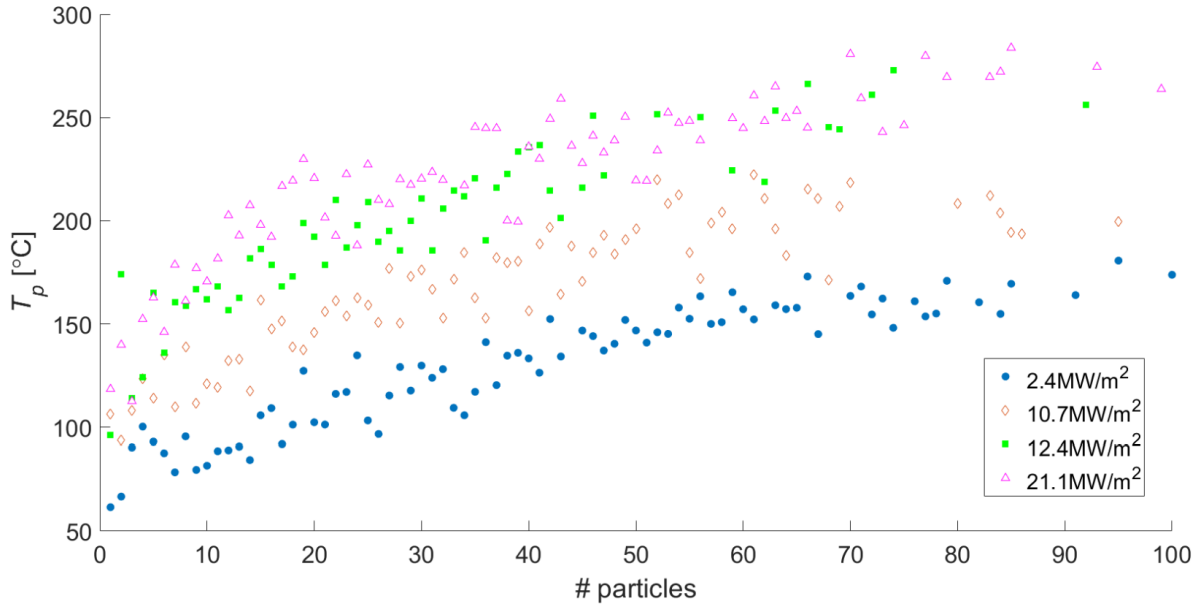

Fig. 6: Dependence of particle temperature on the number of particles per image at Φ = 2.4 MW/m^2, 10.7 MW/m^2, 12.4 MW/m^2 and 21.1 MW/m^2.

4. Conclusion

A direct, non-intrusive planar temperature measurement of radiatively heated fluidised particles has been demonstrated. The technique was found to have an accuracy of ±1% in the calibration experiment, while the application of of it in moving particles presented an accuracy of ±10% in temperatures, where the variation is attributed, mainly to noise from the ICCD camera. A clear dependence of particle temperature on heat flux and particle mass loading was found.

Acknowledgement

We gratefully acknowledge support from the Australian Research Council through its Discovery grant 150102230 and Linkage Grant LE130100127.
The authors would also like to thank Mr Jeffrey Hiorns and Mr Jason Peak, from the mechanical workshop at the School of Chemical Engineering, for their outstanding technical support. The financial support from the Institute or Mineral and Energy Resource (IMER) and the Faculty of Engineering, Computer & Mathematical Science (ECMS) at The University of Adelaide is acknowledged.

References

Abram, C., Fond, B., Beyrau, F., 2015. High-precision flow temperature imaging using ZnO thermographic phosphor tracer particles. Optics Express 23, 19453-19468.
Abram, C., Fond, B., Heyes, A.L., Beyrau, F., 2013. High-speed planar thermometry and velocimetry using thermographic phosphor particles. Applied Physics B: Lasers and Optics 111, 155-160.
Aldén, M., Omrane, A., Richter, M., Sarner, G., 2011. Thermographic phosphors for thermometry: A survey of combustion applications. Progress in Energy and Combustion Science 37, 422-461.
Alwahabi, Z.T., Kueh, K.C.Y., Nathan, G.J., Cannon, S., 2016. Novel solid-state solar thermal simulator supplying 30,000 suns by a fibre optical probe. Optics Express 24, A1444-A1453.
Chen, H., Chen, Y., Hsieh, H.-T., Siegel, N., 2006. Computational Fluid Dynamics Modeling of Gas-Particle Flow Within a Solid-Particle Solar Receiver. Journal of Solar Energy Engineering 129, 160-170.
Denholm, P., Wan, Y.-H., Hummon, M., Mehos, M., 2013. An Analysis of Concentrating Solar Power with Thermal Energy Storage in a California 33% Renewable Scenario, in: NREL (Ed.), Colorado.
Fond, B., Abram, C., Heyes, A.L., Kempf, A.M., Beyrau, F., 2012. Simultaneous temperature,mixture fraction and velocity imaging in turbulent flows using thermographic phosphor tracer particles. Optics Express 20, 22118-22133.
Gil, A., Medrano, M., Martorell, I., Lázaro, A., Dolado, P., Zalba, B., Cabeza, L.F., 2010. State of the art on high temperature thermal energy storage for power generation. Part 1—Concepts, materials and modellization. Renewable and Sustainable Energy Reviews 14, 31-55.

Grena, R., 2009. Thermal simulation of a single particle in a falling-particle solar receiver. Solar Energy 83, 1186-1199.
Hasegawa, R., Sakata, I., Yanagihara, H., Johansson, B., Omrane, A., Aldén, M., 2007. Two-dimensional gas-phase temperature measurements using phosphor thermometry. Applied Physics B: Lasers and Optics 88, 291-296.
IEA, 2014. Technology Roadmap - Solar Thermal Electricity. 4.
Jovicic, G., Zigan, L., Will, S., Leipertz, A., 2015. Phosphor thermometry in turbulent hot gas flows applying Dy:YAG and Dy:Er:YAG particles. Measurement Science and Technology 26.
Kreith, F., Goswami, D.Y., 2007. CRC Handbook of Energy Efficiency and Renewable Energy. Taylor and Francis.
Kueh, K.C.Y., Lau, T.C.W., Nathan, G.J., Alwahabi, Z.T., 2017. Single-shot Planar Temperature Imaging of Radiatively-heated Fluidized Particles Optics Express.
Kuravi, S., Trahan, J., Goswami, D.Y., Rahman, M.M., Stefanakos, E.K., 2013. Thermal energy storage technologies and systems for concentrating solar power plants. Progress in Energy and Combustion Science 39, 285-319.
Lau, T.C., Nathan, G.J., 2016. The effect of Stokes number on particle velocity and concentration distributions in a well-characterised, turbulent, co-flowing two-phase jet. Journal of Fluid Mechanics 809, 72-110.
Lau, T.C.W., Nathan, G.J., 2017. A method for identifying and characterising particle clusters in a two-phase turbulent jet. International Journal of Multiphase Flow 88, 191-204.
Monchaux, R., Bourgoin, M., Cartellier, A., 2012. Analyzing preferential concentration and clustering of inertial particles in turbulence. International Journal of Multiphase Flow 40, 1-18.
Särner, G., Richter, M., Aldén, M., 2008. Investigations of blue emitting phosphors for thermometry. Measurement Science and Technology 19.
Wang, F., Bai, F., Wang, T., Li, Q., Wang, Z., 2016. Experimental study of a single quartz tube solid particle air receiver. Solar Energy 123, 185-205.